A Relation between the G-R *b*-value and Spatial Fractal Dimensions and Entropy

F. A. Nava

Centro de Investigación Científica y Educación Superior de Ensenada, Baja California (CICESE).

Corresponding author: F. Alejandro Nava

fnava@cicese.mx

Centro de Investigación Científica y Educación Superior de Ensenada, Baja California, Carretera Ensenada – Tijuana No. 3918, Zona Playitas, C.P. 22860, Ensenada, B.C., México.

ORCID: 0000-0001-6778-2017

Abstract

Measurements of the fractal dimensions and entropy of the spatial distribution of seismic sources correlate with measurements of the Gutenberg-Richter *b*-value but, although this parameter is related to the fractal dimension of the rupture areas distribution and to the entropy of the magnitude distribution, there is no clear mechanism to relate it to epi- or hypocentral source distributions. A plausible relation between the *b*-value and the spatial source distributions is proposed and tested through Monte Carlo simulation on a cellular automaton model based on the premise that the probability of an earthquake occurring at a particular point in space is proportional to the stress at that point. Results showing the appropriate correlations are robust and not critically dependent on the values of the parameters of the model.

Keywords: Gutenberg-Richter *b*-value, spatial fractal dimensions, spatial entropy, cellular automata, Monte Carlo simulation

Statements and Declarations

There are no financial or personal competing interests that are directly or indirectly related to the work submitted for publication.

Introduction

A parameter widely used to characterize magnitude distributions is the *b*-value of the Gutenberg-Richter (G-R) relation (Ishimoto & Ida, 1939; Gutenberg & Richter, 1944, 1954)

$$\log_{10} N(M) = a - b\,(M - M_c); \quad M \geq M_c \tag{1}$$

where $N(M)$ is the number of magnitudes $\geq M$, M_c is the completeness magnitude, the threshold above which all events are detected, $N(M_c) = 10^a$ is the total number of data, and the *b*-value, which will be referred to henceforward as simply *b*, determines the proportion of large magnitudes to small ones (Richter, 1958). The G-R relation (1) is a reverse cumulative histogram, usually consisting of magnitudes rounded to ΔM, corresponding to an exponential magnitude probability density function,

$$p(m) = \beta\, \mathrm{e}^{-\beta\,(m - m_c)}\,, \tag{2}$$

where

$$\beta = \, b \ln(10) = 1/(\mu - m_c)\,, \tag{3}$$

μ is the mean of the exponential distribution, and (2) is defined for unrounded magnitudes $m \geq m_c = M_c - \frac{\Delta M}{2}$, and usually $\Delta M = 0.1$.

The importance of b cannot be overemphasized because it is inversely related to the level of stress in a region (Scholz, 1968; Schorlemmer et al., 2005, El-Isa, Z., Eaton, D. (2014), Scholz, 2015), which makes it useful for detecting magma chambers (Wiemer & McNutt, 1997; Wyss, 1973; Wyss et al., 1997; Farías et al., 2023) and invaluable as a seismic precursor to large earthquakes, because it has been found to decrease before large earthquakes (e.g. Hirata, 1989; Ouchi and Uekawa, 1986; Dimitriu et al., 2000; Enescu & Ito, 2001; Nuannin et al., 2005; Nanjo et al., 2012; Sharma et al., 2013; Gulia et al., 2016; Wang, 2016; Wang et al, 2016; Borgohain et al., 2018; Li & Chen, 2021; Trifonova et al, 2024).

A second observable used to characterize distributions is the fractal dimension; fractal distributions obey a power relation

$$N = \frac{C}{r^D}, \tag{4}$$

where N is the number of objects measured with a characteristic linear dimension r, C is a proportionality constant, and D is the fractal dimension (Mandelbrot, 1967, 1983; Turcotte, 1989, 1997; Goltz, 1997).

Based on the exponential distribution of magnitudes and the logarithmic relation between magnitudes and seismic moments that has slope c, with $c = 1.5$ (Hanks and Kanamori, 1979), and the approximate relation between seismic moment M_0 and rupture area A

$$M_0 = \alpha A^{3/2} \tag{5}$$

proposed by Kanamori and Anderson (1975), Aki (1981) proposed the relation

$$D = \frac{3b}{c} = 2b \tag{6}$$

between the fractal dimension D of the seismic rupture areas and b (see Turcotte (1997) for a nice derivation of (6)). But this relation does not refer to the spatial distribution of earthquakes or its fractality. Indeed, Hirata (1989) measured epicentral fractal dimensions and found that they do not agree with (6), while Wyss et al. (2004) find that (6) could be (very) approximately satisfied for a locked region near Parkfield.

However, several studies have found that epicentral or hypocentral space distributions present fractal behavior (e.g., Goltz, 1977) and are, like most natural fractal phenomena, multifractal (e.g., Goltz, 1977; Turcotte, 1989; Geilikman et al., 1990; Hirabayashi et al., 1992). Furthermore, changes in fractal dimensions have been observed before large earthquakes (Dongsheng et al., 1994; Dimitriu et al., 2000; Enescu and Ito, 2001; Bhattacharya et al., 2002; Márquez et al., 2012; Márquez-Ramírez, 2012), which gives precursory importance to measuring epicentral or hypocentral fractal dimensions. Huang and Turcotte (1988) present a model that simulates a 2D planar fault zone where the difference between stress and strength follows a fractal distribution and find that b correlates positively with the fractal dimension.

A third observable used to characterize distributions is the Shannon (1948) entropy,

$$S = -\sum_{k=1}^{K} P_k \log_2 P_k \,, \tag{7}$$

where P_i is the probability corresponding to element or class i, there are K elements, and

$$\sum_{k=1}^{K} P_k = 1 \,. \tag{8}$$

The logarithm can have any base; but base 2 is the one most commonly used for information purposes and yields an entropy expressed in bits, easy to interpret. The entropy, equal to the expected self-information (Fano, 1961), is a measure of the uncertainty in the distribution and can be measured against the entropy of a uniform distribution where $p_k = p_u = 1/K$ and $S_U = \log_2 K$.

The entropy of the magnitude distribution with parameter β and class width ΔM, is related to $b = \beta \ln 10$ as

$$S = \beta\, \Delta M \, \frac{\mathrm{e}^{-\beta\, \Delta M}}{1 - \mathrm{e}^{-\beta\, \Delta M}} \log_2 \mathrm{e} - \log_2\!\left(1 - \mathrm{e}^{-\beta\, \Delta M}\right) \tag{9}$$

(Nava, 2024), where the commonly used $\Delta M = 0.01$ can be considered a fixed, constant value.

It should be noted that relation (9) between b and entropy refers to the entropy of the magnitude distribution itself and does not refer to the spatial distribution of epi- or hypocenters of an earthquake data set.

The entropy of the spatial distribution of epicenters has been used as a measure of how “ordered” is this distribution (e.g., Bressan et al., 2017; Goltz, 1966; Goltz and Böse, 2002; Nava et al., 2021; Nicholson et al., 2000; Ohsawa, 2018), while other studies relate entropy as a measure of proximity to criticality (Rundle et al. 2019; Main and Al-Kindy, 2002; Sarlis et al, 2018; Vogel et al, 2020; Varotsos et al., 2023)

Since both the spatial fractal dimensions and the spatial entropy of epicentral spatial distributions correlate with b (e.g., Chen et al, 2006; Roy et al., 2010), there must be a reason why b values are reflected in the characteristics of the spatial epicentral distributions. In the present paper we propose a possible mechanism that relates these three quantities, and we explore its possibilities through Monte Carlo simulations.

The model

Since both epicentral and hypocentral distributions are observed to correlate with *b,* and epicentral locations are less uncertain than hypocentral ones, a 2D model, easily extended to 3D, will be considered here. Hence, we will refer to the spatial distribution of seismic sources as an epicentral distribution.

The model is a cellular automaton consisting of a grid that divides the study area into cells; the grid defines two matrices of dimensions $N_i \times N_j$, one containing the number of events occurring within each cell and the other containing the stress in each cell. The model operates based on the following premises:

I. Each earthquake will rupture an area exponentially proportional to the magnitude and will release the stress in the ruptured area. The remanent stress can have some non-zero low value but as will be shown, this value is not very important, so we will consider it to be zero.

This premise derives from the relation between seismic moment and rupture area A

$$M_0 = \mu \bar{d} A \, , \tag{10}$$

where μ is the rigidity and $\bar{d}$ is the average slip on the fault (Aki, 1966). This relationship is also observed empirically; in their classic paper Wells and Coppersmith (1994) (W-C) find $A = 10^{a+cM}$ with $a \sim -3.5$ and $c \sim 0.9$.

Hence rupture area A and unrounded magnitudes m will be related as

$$A = C\, e^{\alpha(m-m_c)}\,, \tag{11}$$

where m_c is the minimum unrounded magnitude α and C are constants. We will use $\alpha = 1.7$, which corresponds approximately to the c in W-C; setting $C = 1$ defines a unit rupture area for the minimum magnitude, and we will consider this the area of one cell in the automaton, which would be ~0.16 km^2 (W-C). Since we will be using $N_i = 40$ and $N_j = 50$, an event with $M \sim 7.4$ would rupture almost all 2,000 cells, so we will use $m_{max} = 7.4$.

Since A is a real number and the number of ruptured cells must be an integer, the number of ruptured cells will be calculated as

$$\begin{gathered} A_c = n_i \times n_j\,, \\ n_i = \mathrm{Fix}\left(\sqrt{A}\right), \\ n_j = \mathrm{Round}(A/n_i) \end{gathered} \tag{12}$$

We calculated first the number in the i dimension because we will be using $N_j > N_i$ and errors will be smaller this way. Figure 1 shows A and A_c as a function of the magnitude M for $\alpha = 1.7$ and, since the lines are almost undistiguishable the error $A - A_c$ and the relative error $\frac{(A-A_c)}{A}$ are also shown. The n_i and n_j cells will be centered (as far as possible) around the cell where the earthquake occurred.

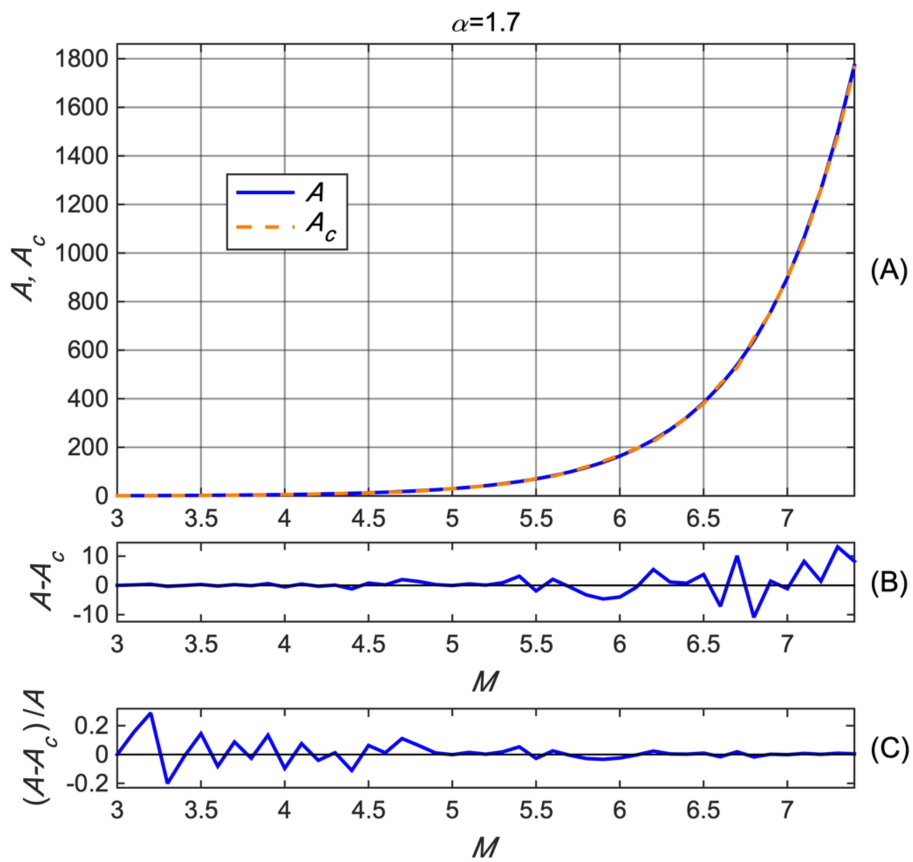

Figure 1. Rupture area A and rupture cell area A_C as a function of magnitude (A). The error $A - A_C$ is shown in (B), and the relative error $(A - A_C)/A$ is shown in (C).

II. Each earthquake will cause stress concentrations on the borders of the rupture. One unit of stress will be added to each cell around the rupture. Since only the relative values of stress will be used, it is not necessary to assign any constant or proportionality or particular units to the stress.

The first two premises are illustrated in Figure 2 that shows the occurrence of three earthquakes on a surface with uniform stress. The panel on the left shows the earthquake locations and the right-hand side panel shows the stresses. The event at $i = 30, j = 12$ is an $M = 3.0$ that ruptures one cell; at $i = 20, j = 30$ is an $M = 5.5$, and on its border, at $i = 15, j = 25$, occurred an $M = 4.5$ event that released the left-hand corner stress concentrations due to the previous earthquake and increased the stresses where the borders intersect.

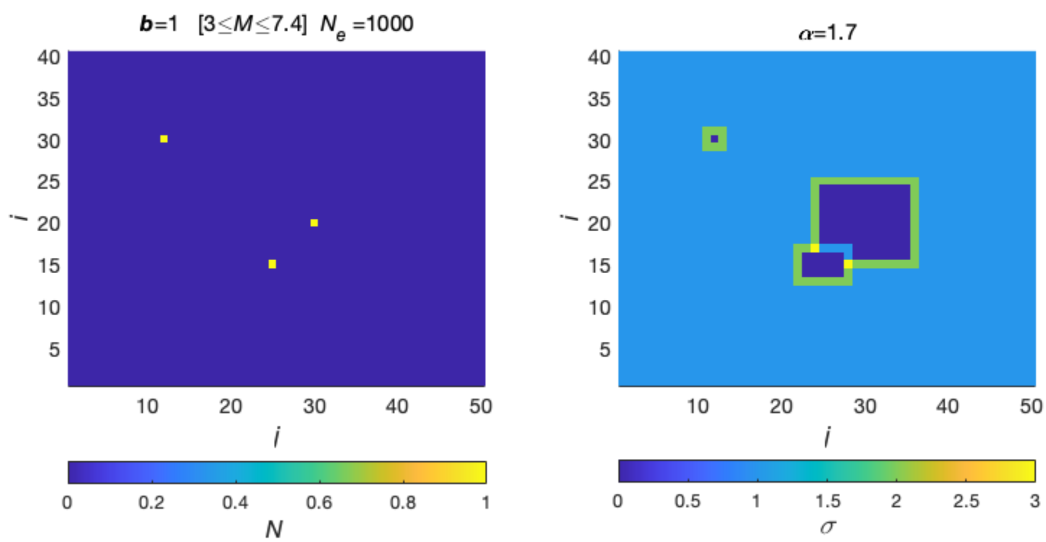

Figure 2. Examples of the effects of the occurrence of earthquakes on the location (left) and stress (right) matrices of the automaton (see text for explanation).

III. The third premise is the key to the fractal location of the epicenters; we heuristically propose that each earthquake location, i.e., the cell to which an earthquake is assigned, should be randomly chosen with probabilities proportional to the stress in each cell. The epicentral location will be the center of the cell.

Thus, for each realization a set of $N_T = N_0 + N_e$ magnitudes between m_c and m_x is generated according to (2). The first N_0 events are used to *prime* an initially uniform stress field matrix, and the locations of the following N_e events are recorded in the number-of-events matrix (the *catalog*).

To determine which cell will host an event, a cumulative sum of all current stresses is calculated and normalized to one, a uniformly distributed random number in the [0,1] range is generated and a search is made for the cell corresponding to the random value (actually, instead of doing $N_i \times N_j$ divisions, the random number is multiplied by the largest cumulative value and then compared with the non-normalized cumulative).

Figure 3 shows the results of a realization with $N_0 = 500$ and $N_e = 1{,}000$ events for $b = 0.8$. Panel (A) shows a histogram of the N_T exponentially distributed magnitudes, panel (B) shows the spatial distribution of the N_e epicenters, and panel (C) shows the spatial distribution of stresses at the end of the realization, stresses distributed in size as shown in (D).

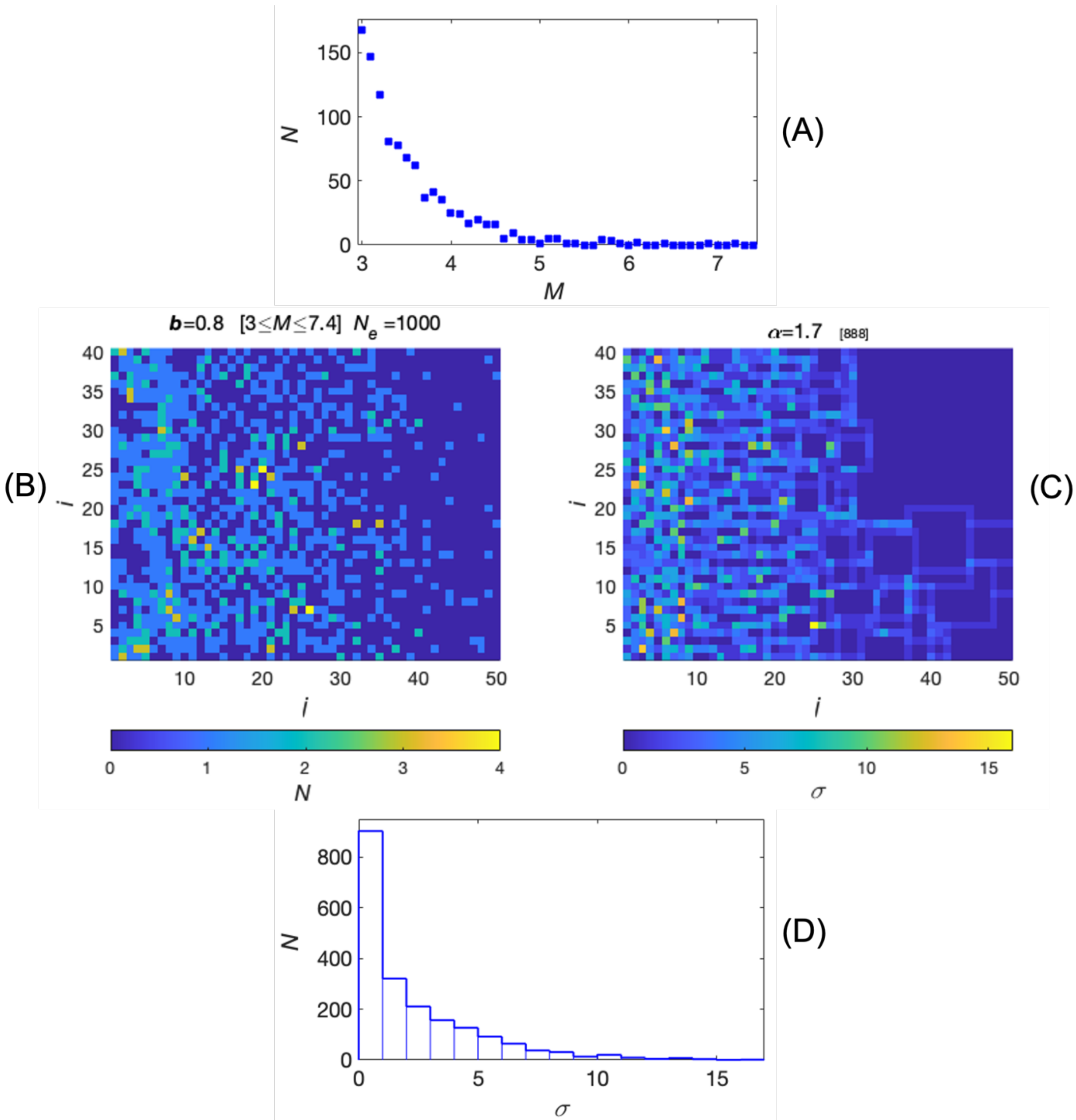

Figure 3. Example of a realization of $N_T = 1500$ events with magnitudes for $b = 0.8$ distributed as shown in (A) and the resulting spatial distribution of $N_e = 1{,}000$ epicenters (B) and of the dimensionless stress (C). The small number in brackets above (C) is the seed of the random number generator.

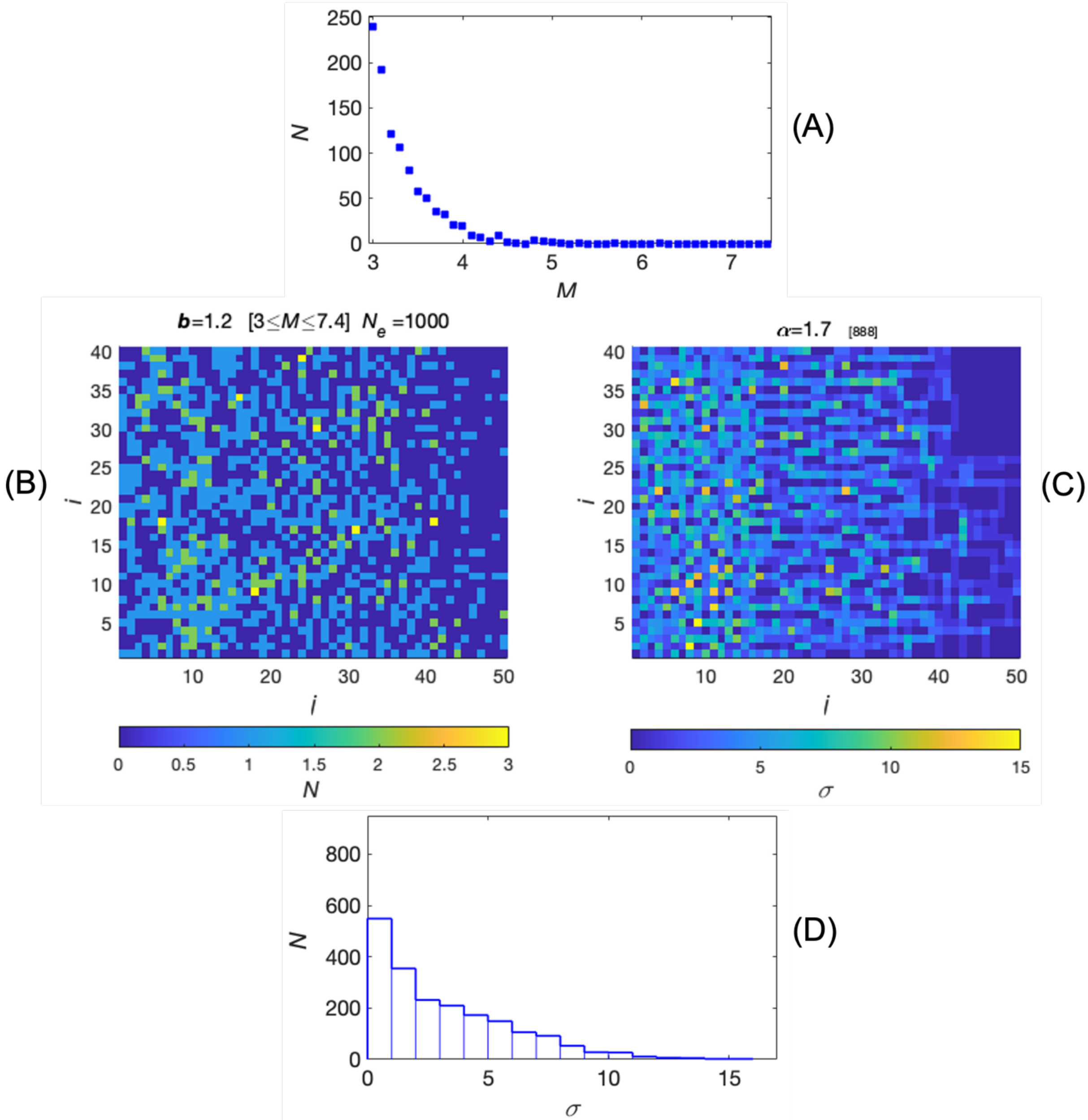

Figure 4. Example of a realization of $N_T = 1500$ events with magnitudes for $b = 1.2$ distributed as shown in (A) and the resulting spatial distribution of $N_e = 1{,}000$ epicenters (B) and the dimensionless stress (C). The small number in brackets above (C) is the seed of the random number generator.

Figure 4 shows the same features as Figure 6, for $b = 1.2$; the stress histogram in (D) has been plotted using the same scales as the corresponding one in Figure 3 to show the differences between them. The realizations shown in Figures 3 and 4 both used the same series of pseudo-random numbers, so all differences are due only to the difference in b.

For each realization, fractal dimensions and entropy are measured on the spatial epicentral distribution as described below.

Most natural fractal phenomena are not monofractal (Turcotte, 1989; Geilikman et al., 1990; Hirata and Imoto, 1991; Hirabayashi et al., 1992) so fractal measures that count the number of neighbors around a point or a source in different ways, result in different dimension estimates.

Here, we will calculate the fractal dimensions following the methods described in Grassberger and Procaccia (1983a), Pawelzik and Schuster (1987a,b), Harte (2001), and others that, based on Rényi's (1961) information measures, define the q'th order dimension as

$$D_q = \frac{1}{q-1} \lim_{r \to \infty} \frac{\log C_q(r)}{\log r} \approx \frac{\phi_q}{q-1}\ , \tag{13}$$

where q is the order, r is the size, and ϕ_q is the slope of the linear fit to the $\log C_q(r)$ vs. $\log r$ plot.

$$C_q(r) = \lim_{N \to \infty} \frac{1}{N} \sum_{i=1}^{N} \left[\frac{1}{N-1} \sum_{j \neq i} \mathrm{H}\left(r - \left|x_i - x_j\right|\right) \right]^{q-1} \propto r^{D_q} \tag{14}$$

is the correlation integral (Hentschell and Procaccia, 1983; Pawelzik and Schuster, 1987a, b; Grassberger & Procaccia, 1993; Grassberger, P. (2007)).

Since (13) cannot be used for $q = 1$, D_1 is calculated from

$$D_1 = \lim_{r\to 0} \frac{\lim_{N\to\infty} \frac{1}{N} \sum_{i=1}^{N} \log\left[\frac{1}{N-1} \sum_{j\neq i} \mathrm{H}\left(r - |x_i - x_j|\right)\right]}{\log r} \quad (15)$$

(see details in Márquez et al., 2012).

Although q can range from $-\infty$ to ∞, the dimensions for $q > 0$ are the ones emphasizing denser regions and those for small q are the most sensitive (Hirabayashi et al, 1992). We will not measure D_0 because this measure is not appropriate for working with cells (unless there is an enormous number of them) because all events corresponding to any one cell are located at exactly the same point.

For the example shown in Figure 3, for $b = 0.8$, $D_1 = 0.9428$, and $D_2 = 0.9049$, while for the example for $b = 1.2$, shown in Figure 4, $D_1 = 1.0575$, and $D_2 = 1.0436$, both dimensions larger than the corresponding ones for $b = 0.8$.

To compute the entropy, the probability for cell $k = (i-1)N_i + j$ is estimated as

$$p_k = \frac{n_k}{N}, \quad (16)$$

so condition (8) is fulfilled, and formula (7) is applied. Note that null probabilities do not contribute to the entropy.

A reference value is the entropy for a uniform distribution; if probability were the same for all cells, then

$$S_U = -\sum_{k=1}^{N_{xy}} \frac{1}{N_{xy}} \log_2 \frac{1}{N_{xy}} = \log_2 N_{xy}$$

$$S_U = 10.9658$$

For the examples shown above $S = 9.544$ bit for $b = 0.8$, and is smaller than $S = 9.5745$ bit, for $b = 1.2$.

For any given parameter set, results vary slightly for different pseudo-random number series (generated using different 'seeds' in the Matlab *rand.m* algorithm), so we use Monte Carlo simulation to do $N_r = 200$ realizations of any given parameter set for *b* values in the 0.8 to 1.2 range (Bhattacharya et al. (2002) report an observed range from 0.7 to 1.3) to see whether the mean values of the fractal dimensions and the entropy show a particular behavior depending on *b*.

The same pseudo-random number series and the same parameter sets are used for each *b* value, so the different values of dimensions and entropy resulting for different *b* values are only due to the differences in *b*.

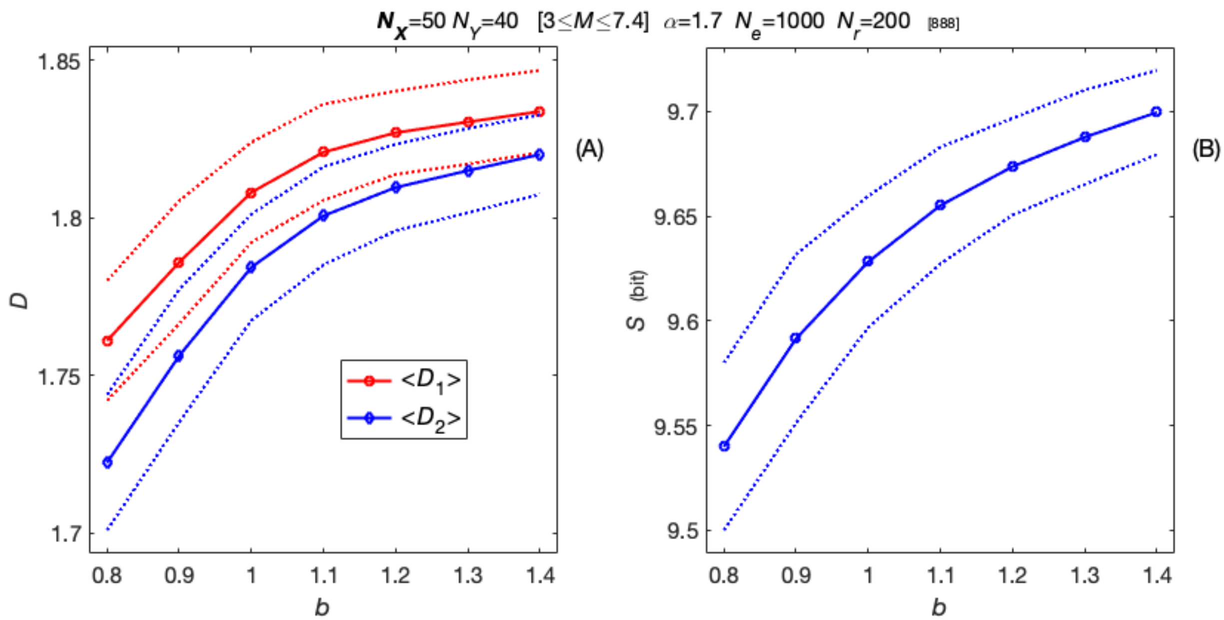

Figure 5. For the parameter set shown in the title (the small number within brackets is the pseudo-random number generator seed), panel (A) shows mean epicentral fractal dimensions $< D_1 >$ and $< D_2 >$ as solid lines, the dotted lines indicate $< D_1 > \pm s_{D_1}/2$ and $< D_2 > \pm s_{D_2}/2$, where s_{D_1} and s_{D_2} are the standard deviations of D_1 and D_2, respectively. The solid line in (B) is the mean entropy $< S >$ and the dotted lines indicate $< S > \pm s_S$, where s_S is the standard deviation of S.

Our principal result is shown in Figure 5 that clearly illustrates that the means (solid lines with markers) of both the fractal dimensions D_1 and D_2 (A) and of the entropy S (B) correlate nicely with b. Although the standard deviations are large, particularly for the fractal dimensions, clearly results for low b differ from those for high b. Multifractality, the difference between the different dimension measures D1 and D2 (Dimitriu et al, 2000), also increases slightly as b decreases.

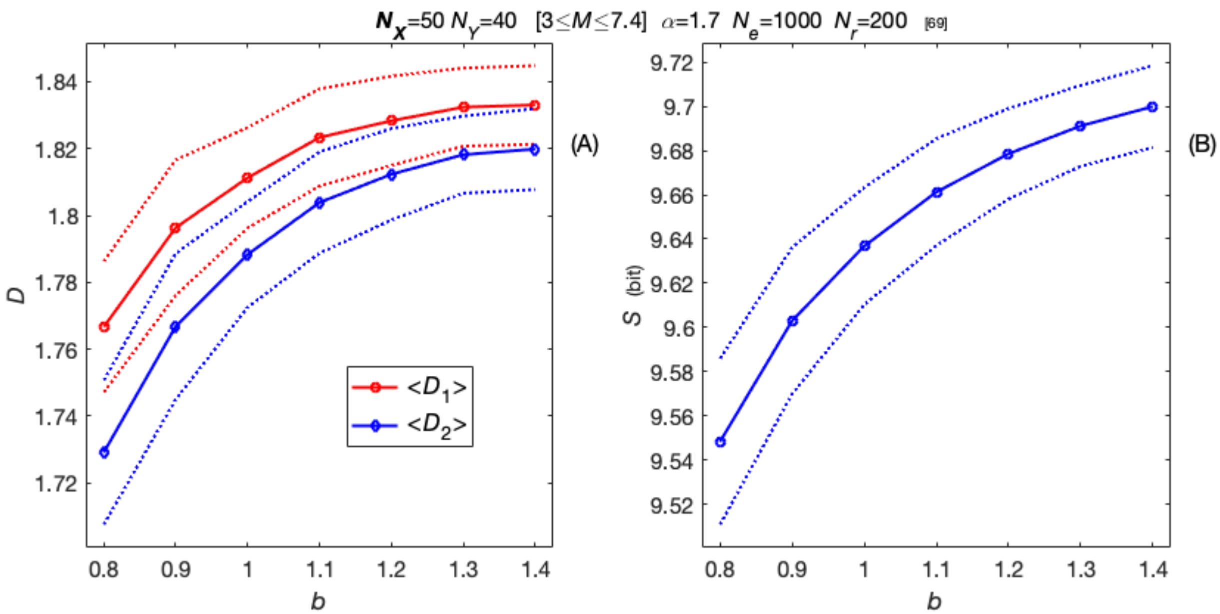

Figure 6. Same parameter set as in Figure 5 but using a different seed shown within brackets in the title. All conventions are the same as in Figure 5.

An immediate question is whether the results shown above are an isolated or unique result due to a particular parameter set, and the answer is a rotund 'No'. Although details vary for different seeds or parameter sets and the resulting curves can be somewhat less smooth (particularly the fractal dimensions ones) than the ones shown in Figure 5, varying parameter sets or seeds result all in similar behaviors of dimensions and entropy with respect to b.

To illustrate this assertion, Figure 6 shows the results of using the same parameter set shown in Figure 5 but using a different seed. Figure 7 shows results for the same parameter set and seed of Figure 5, except for a lower $\alpha = 1.5$. Figure 8 shows results for a different grid having 45×45 cells instead of the 50×40 of Figure 5. Clearly, different combinations of parameters or different random number series all show very similar behaviors of dimensions and entropy with respect to *b*.

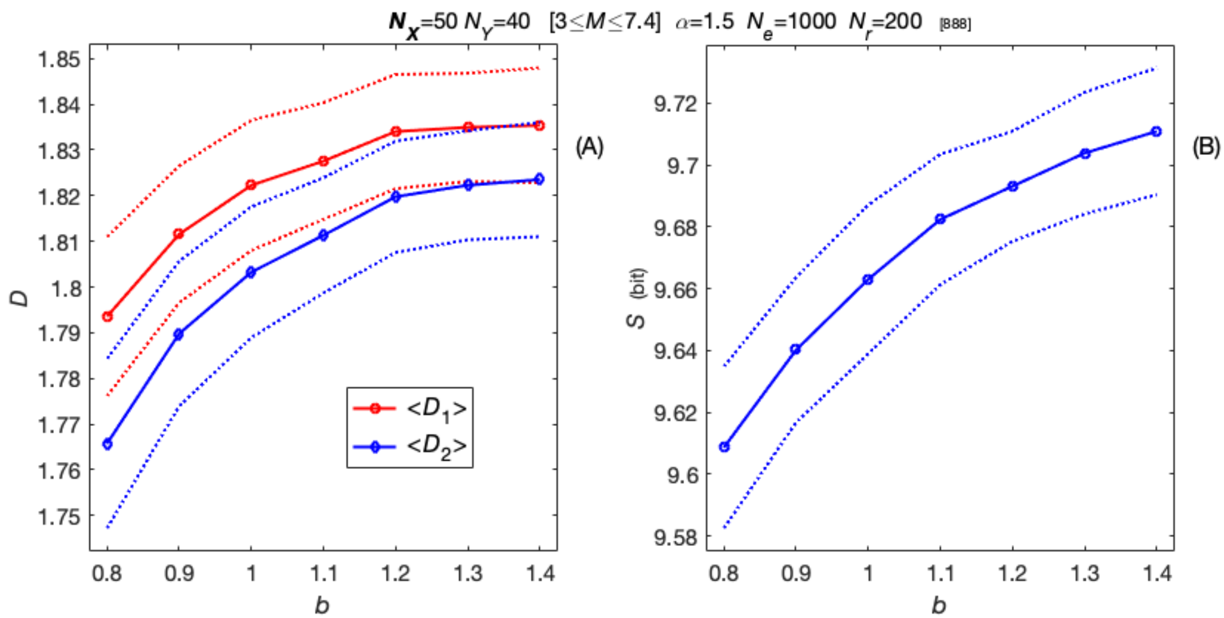

Figure 7. Same parameter set as in Figure 5, except for $\alpha = 1.5$. All conventions are the same as in Figure 5.

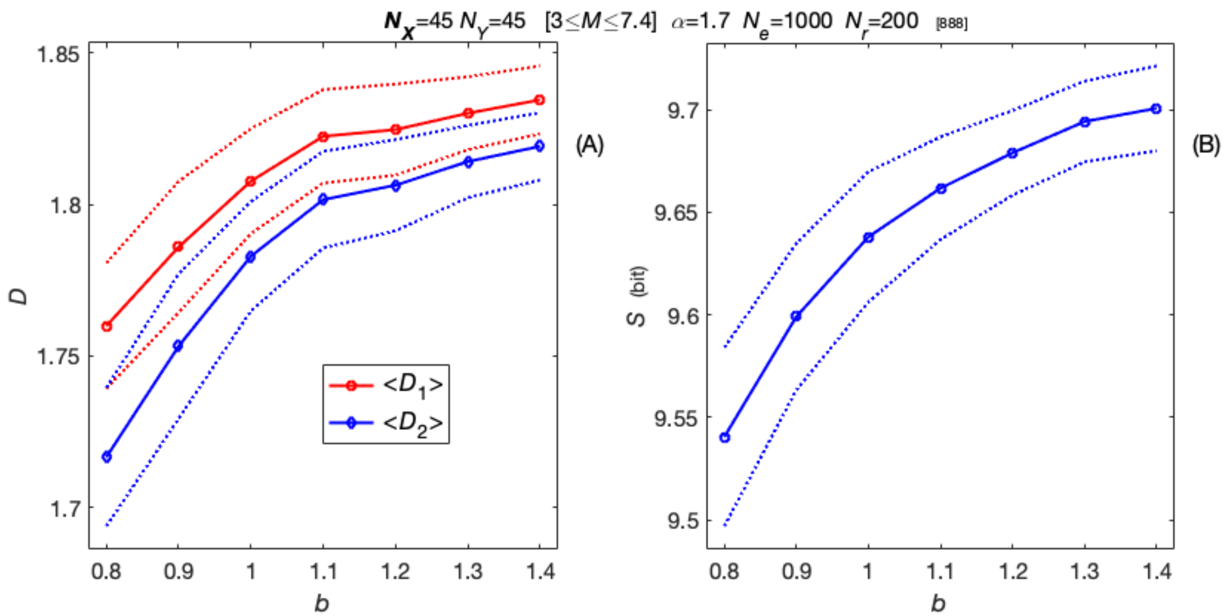

Figure 8. Same set of parameters as in Figure 5, except for a different shape of 45 × 45 cells. All conventions are the same as in Figure 5.

Discussion

We present a very simple model based on the two commonplace assumptions: first, that the rupture area of and earthquake is related exponentially to the magnitude and that the stress in the rupture area is decreased; second, that the rupture will cause increased stress near its borders, plus a third quite reasonable assumption that the probability of an earthquake occurring at a particular place is proportional to the stress in it. The resulting spatial distribution of epicenters presents both multifractal and entropy behavior that positively correlates with the magnitude *b*-values.

The model is a cellular automaton and Monte Carlo simulations are employed to ensure that results are not dependent on any particular set of parameters and/or pseudo-random numbers.

Results are quite robust and do not largely depend on any parameter value; all results for different parameter sets and random numbers show the correlation between fractal dimensions and entropy with *b*.

It should be mentioned that Huang and Turcotte (1988) modeled a relation between a postulated fractal distribution of the difference between stress and strength in a planar 2D mesh, where earthquakes occurred when a critical value of the difference was reached, with *b*; but it is a very different model from the one presented here. They postulated the stresses and strengths together with their fractal distribution and obtained *b* as a result. In our much simpler model, we start from a realistic, commonplace *b* distribution and by assuming the location proportional to the stress obtain fractal epicentral distributions.

We do not claim to have found the one true mechanism that relates *b* with the fractal dimensions and entropy of spatial epicentral distributions, but we present a reasonable, simple, and straightforward mechanism that gives results that agree well with the observed behavior of these quantities.

References

Aki K (1966) Generation and propagation-of G-waves from the Niigata earthquake of June 16, 1964. Part 2: Estimation of earthquake moment, released energy, and stress-strain drop from the G-wave spectrum. Bull. earthq. Res. Inst. 44:73-88. [N/A]

Aki K (1981) A probabilistic synthesis of precursory phenomena. In: Earthquake prediction and international review, Simpson D and Richards P (eds), Am Geophys U, pp 566-574.

Bhattacharya P, Majumdar R, Kayal J (2002) Fractal dimension and *b*-value mapping in northeast India. Curr. Sci. 82: 1486-1491.

Borgohain J, Borah K, Biswas R, Bora D (2018) Seismic *b*-value anomalies prior to the 3rd January 2016, M_W=6.7 Manipur earthquake of northeast India. Journal of Asian Earth Sciences 154: 42-48.

Bressan G, Barnaba C, Gentili S, Rossi G (2017) Information entropy of earthquake populations in northeastern Italy and western Slovenia. Pure Appl. Geophys. 271: 29–46. https://doi.org/10.1016/j.pepi.2017.08.001

Chen C, Wang W, Chang Y, Wu Y, Lee Y (2006) A correlation between the b-value and the fractal dimension from the aftershock sequence of the 1999 Chi-Chi, Taiwan, earthquake. Geophysical Journal International 167: 1215-1219.

Dimitriu P, Scordilis E, Karacostas V (2000) Multifractal analysis of the Arnea, Greece seismicity with potential implications for earthquake prediction. Natural Hazards 21: 277-295.

Dongsheng L, Zhaobi Z, Binghong W (1994) Research into the multifractal of earthquake spatial distribution. Tectonophysics 233: 91-97.

El-Isa Z, Eaton D (2014) Spatiotemporal variations in the b-value of earthquake magnitude–frequency distributions: Classification and causes. Tectonophysics 615: 1–11. doi:10.1016/j.tecto.2013.12.001

Enescu B, Ito K (2001) Some premonitory phenomena of the 1995 Hyogo-Ken Nanbu (Kobe) earthquake: seismicity, b-value and fractal dimension. Tectonophysics 338: 297-314.

Fano R (1961) Transmission of information. M.I.T Press and J. Wiley & Sons, USA, 389pp.

Farías C, Lazo J, Basualto D, Saavedra M, Muñoz-Quiroz F, Zúñiga-Urrea L, Martínez-Bravo R, Huentenao-Inostroza I, Sáez-Opazo R (2023) One decade of b-value variations from volcano-tectonic seismicity as an early indicator of episodes of crisis in a volcano: the case of Copahue, Southern Andes. Frontiers in Earth Science 11: 1181177.

Geilikman M, Golubeva T, Pisarenko V (1990) Multifractal patterns of seismicity. Earth Plan.Sci.Letts. 99: 127-132.

Goltz C (1996) Multifractal and entropic properties of landslides in Japan. Geol Rundsch 85: 71–84.

Goltz C. (1997) Fractal and chaotic properties of earthquakes. Springer-Verlag, Lecture notes in Earth sciences, . ISSN: 0930-0317, DOI: 10.1007/BFb0028315, ISBN: 978-3-540-64893-2.

Goltz C, Böse M (2002) Configurational entropy of critical earthquake populations. Geophys. Res. Lett. 29: 51 - 1-4. DOI: 10.1029/2002GL015540

Grassberger P, Procaccia I (1983a) Characterization of Strange Attractors, Physical Review Letters 50: 346–349.

Grassberger P, Procaccia I (1983b) Measuring the strangeness of strange attractors, Physica D, 9: 189–208.

Grassberger P (2007) Grassberger-Procaccia algorithm. Scholarpedia, 2: 3043.

Gulia L, Tormann T, Wiemer S, Herrmann M, Seif S (2016) Short-term probabilistic earthquake risk assessment considering time-dependent *b*-values. Geophys. Res. Lett. 43: 1100-1108. https://doi.org/10.1002/2015GL066686

Gutenberg B, Richter C (1944) Frequency of earthquakes in California. Bull Seismol Soc Am 34: 185–188.

Gutenberg B, Richter C (1954) Seismicity of the Earth and Associated Phenomena. Second ed., Princeton University Press, Princeton.

Hanks T, Kanamori H (1979) A moment magnitude scale. Journal of Geophysical Research 84: (B5) 2348-2350.

Harte D (2001) Multifractals Theory and Applications. Chapman & Hall/CRC, New York, 2001.

Hentschel H, Procaccia I (1983) The infinite number of generalized dimensions of fractals and strange attractors. Physica D 8: 435–444.

Hirabayashi T, Ito K, Yoshii T (1992) Multifractal analysis of earthquakes. Pure Appl. Geophys. 138: 591-610.

Hirata T (1989) A correlation between the b value and the fractal dimension of earthquakes. *Journal of Geophysical Research:* Solid Earth 94: (B6), 7507-7514.

Hirata T, Imoto M (1991) Multifractal analysis of spatial distribution of microearthquakes in the Kanto region, Geophys. J. Int. 107: 155–162.

Huang J, Turcotte D (1988) Fractal distribution of stress and strength and variations of b-value. Earth Planet. Sci. Lett. 91: 223–230.

Ishimoto M, Iida K (1939) Observations sur les séismes enregistrés par le micro-séismographe construit dernièrement (1), Bull. Earthquake Res. Inst. Univ. Tokyo 17: 443–478.

Kanamori H, Anderson D (1975) Theoretical basis of some empirical relations in seismology. Bull. Seism. Soc. Am. 65: 1073-1095.

Li Y, Chen X. (2021) Variations in apparent stress and *b* value preceding the 2010 M_W8.8 Bio-Bío, Chile earthquake. Pure Appl. Geophys. 178: 4797-4813. https://doi.org/10.1007/s00024-020-02637-3

Main I, Al-Kindy F (2002) Entropy, energy, and proximity to criticality in global earthquake populations. Geophys. Res. Lett. 29: (7) 1121. DOI:10.1029/2001GL014078.

Mandelbrot B (1967) How long is the coast of Britain? Science **156:** 636-638.

Márquez-Ramírez V (2012) Análisis multifractal de la distribución espacial de sismicidad y su posible aplicación premonitora. Exploración de un posible mecanismo para la fractalidad mediante modelado semiestocástico. PhD Thesis, Programa de Posgrado en Ciencias de la Tierra, Centro de Investigación Científica y de Educación Superior de Ensenada, Baja California, México.

Márquez V, Nava F, Reyes G (2012) Multifractality in seismicity spatial distributions: Significance and possible precursory applications as found for two cases in different tectonic environments. Pageoph 169 (12): 2091-2105. https://doi.org/10.1007/s00024-012-0473-9

Nanjo K, Hirata N, Obara K, Kasahara K (2012) Decade-scale decrease in b value prior to the M9-class 2011 Tohoku and 2004 Sumatra quakes. Geophys. Res. Lett. 39: L20304. https://doi.org/10.1029/2012GL052997

Nava F, Despaigne G, Glowacka E (2021) Poisson renormalized entropy as a possible precursor to large earthquakes. Journal of Seismology 25: 1407-1425. https://doi.org/10.1007/s10950-021-10041-0.

Nava F (2024) Seismic magnitudes entropy and b-value. Acta Geophysica 1-12. https://doi.org/10.1007/s11600-024-01424-1

Nicholson T, Sambridge M, Gudmundsson Ó (2000) On entropy and clustering in earthquake hypocentre distributions. Geophys. J. Int. 142: 37-51.

Nuannin P, Kulhanek O, Persson L (2005) Spatial and temporal *b* value anomalies preceding the devastating off coast of NW Sumatra earthquake of December 26, 2004. Geophys. Res. Lett. 32: L11307. doi:10.1029/2005GL022679.

Ohsawa Y (2018) Regional seismic information entropy to detect earthquake activation precursors. Entropy 20(11): 861.

Ouchi T, Uekawa T (1986) Statistical analysis of the spatial distribution of earthquakes—variation of the spatial distribution of earthquakes before and after large earthquakes. Physics of the Earth and Planetary Interiors 44(3): 211-225.

Pawelzik K, Schuster H (1987a) Generalized dimensions and entropies from a measured time series. Physical Review A, 35(1): 481.

Pawelzik K, Schuster H (1987b) Erratum: Generalized dimensions and entropies from a measured time series [Phys. Rev. A 35, 481 (1987)]. Physical Review A, 36(9): 4529.

Rényi A (1961) On measures of information and entropy. Proceedings of the 4th Berkeley Symposium on Mathematics, Statistics and Probability 1961, 547-561.

Richter C. (1958) Elementary seismology. W. H. Freeman and Co., USA, 768pp.

Roy P, Ghosh U, Hazra S, Kayal J (2010) Fractal dimension and *b*-value mapping in the Andaman-Sumatra subduction zone. Natural Hazards 57: 27-37. DOI 10.1007/s11069-010-9667-6

Rundle J, Giguere A, Turcotte D, Crutchfield J, Donnellan A (2019) Global seismic nowcasting with Shannon information entropy. Earth and Space Science 6 (1): 191-197.

Sarlis N, Skordas E, Varotsos P (2018) A remarkable change of the entropy of seismicity in natural time under time reversal before the super-giant M9 Tohoku earthquake on 11 March 2011. Europhysics Letters 124(2): 29001. https://doi.org/10.1209/0295-5075/124/29001

Scholz C (1968) The frequency-magnitude relation of microfracturing in rock and its relation to earthquakes. Bull. seism. Soc. Am. 58: 399–415. doi: 10.1785/BSSA0580010399.

Scholz C (2015) On the stress dependence of the earthquake *b* value. Geophys. Res. Lett. 42: 1399-1402, doi:10.1002/2014GL062863.

Schorlemmer D, Wiemer S, Wyss M (2005) Variations in earthquake size distribution across different stress regimes. Nature 437: 539–542 doi:10.1038/nature04094.

Shannon C (1948) A mathematical theory of communication. The Bell System Technical Journal 27: 379-423, 623-656.

Sharma S, Saurabh B, Prakash S, Pabon K, Duarah R (2013) Low *b*-value prior to the Indo-Myanmar subduction zone earthquakes and precursory swarm before the May 1995 M 6.3 earthquake. Journal of Asian Earth Sciences 73: 176-183.

Trifonova P, Oynakov E, Popova M, Aleksandrova I (2024) Seismic variations before Eastern Anatolian catastrophic events in February 2023. Natural Hazards 121: 1289-1301. https://doi.org/10.1007/s11069-024-06831-7

Turcotte D (1989) Fractals in geology and geophysics. Pure Appl. Geophys. 131: 171-196.

Turcotte D (1997) Fractals and Chaos in Geology and Geophysics. Cambridge University Press, Second Edition, New York. 221pp.

Varotsos P, Sarlis N, Skordas E, Nagao T, Kamogawa M, Flores-Márquez E, et al. (2023) Improving the Estimation of the Occurrence Time of an Impending Major Earthquake Using the Entropy Change of Seismicity in Natural Time Analysis. Geosciences 13 (8): 222.

Vogel E, Brevis F, Pastén D, Muñoz V, Miranda R, Chian A (2020) Measuring the seismic risk along the Nazca–South American subduction front: Shannon entropy and mutability. Natural Hazards and Earth System Sciences 20(11): 2943-2960.

Wang J (2016) A mechanism causing *b*-value anomalies prior to a mainshock. Bull. Seismol. Soc. Am. 106: 1663-1671, DOI:10.1785/0120150335

Wang J, Chen K, Leu P, Chang C (2016) Precursor times of abnormal *b*-values prior to mainshocks. J. Seismol. online. DOI: 10.1007/s10950-016-9567-7

Wells D, Coppersmith K (1994) New empirical relationships among magnitude, rupture length, rupture width, rupture area, and surface displacement. Bull. Seismol. Soc. Am. 84: 974-1002.

Wiemer S, McNutt S (1997) Variations in the frequency-magnitude distribution with depth in two volcanic areas: Mount St. Helens, Washington, and Mt. Spurr, Alaska. Geophysical Research Letters 24(2): 189-192.

Wyss M (1973) Towards a Physical Understanding of the Earthquake Frequency Distribution. Geophysical Journal of the Royal Astronomical Society 31(4): 341–359. doi: 10.1111/j.1365- 246X.1973.tb06506.x.

Wyss M, Shimazaki K, Wiemer S (1997) Mapping active magma chambers by *b*-value beneath the off-Ito volcano, Japan. J. Geophys. Res. 102: 20413-20422.

Wyss M, Sammis C, Nadeau R, Wiemer S (2004) Fractal dimension and *b*-value on creeping and locked patches of the San-Andreas fault near Parkfield, California, Bull. seism. Soc. Am. 94: 410–421.